# Microscopic mechanisms of giant magnetoresistance

C. Vouille, A. Barthélémy, F. Elokan Mpondo, and A. Fert
*Unité Mixte de Recherche CNRS-Thomson/CSF, 91404 Orsay, France*

P. A. Schroeder, S. Y. Hsu, A. Reilly, and R. Loloee
*Department of Physics and Astronomy, Michigan State University, East Lansing, Michigan 48824*
(Received 22 February 1999)

We present magnetoresistance measurements aimed at answering several open questions in the understanding of giant magnetoresistance (GMR). Our measurements are performed on ($F1/N/F2/N$) multilayers in which $N$ is a nonmagnetic metal (Cu or Cr), and $F1$ and $F2$ are various ferromagnetic metals or alloys. In current perpendicular to the plane (CPP) measurements on ($F1$/Cu/Co/Cu) multilayers, where $F1$ is Fe, Co, or Ni doped with impurities, we observe an inversion of the GMR for V or Cr impurities; this demonstrates, first the importance of the extrinsic effects in GMR and secondly the possibility of obtaining negative as well as positive values of the bulk spin asymmetry coefficient $\beta$. A compensation thickness with zero GMR is found when the bulk and interface spin asymmetry have opposite signs in the same layer. We interpret the sign of $\beta$ in models of electronic structure. Measurements on other series of multilayers allow us to show that the interface spin asymmetry coefficient $\gamma$ can also be positive (interfaces with Cu) or negative (interfaces with Cr). Finally, the comparison between CPP and CIP data obtained on the same samples sheds light on the different role of the interface intrinsic potential in the two geometries. [S0163-1829(99)09133-X]

## I. INTRODUCTION

Although giant magnetoresistance (GMR) is applied nowadays in several devices, its understanding at the microscopic scale is not completely clear yet.[1] There are still a number of pending questions and the objective of the experimental work we report here is to answer some of the most important ones. For example, in order to clearly identify extrinsic contributions coming from spin dependent scattering by imperfections, we have studied the GMR of a series of multilayers doped with impurities; we will see that doping the ferromagnetic layers with a few percent of impurities can strongly influence the GMR and even, in some conditions explained below, change its sign from negative (normal GMR) to positive (inverse GMR). However, we will also see that the GMR cannot be explained by only extrinsic effects (scattering by imperfections); it is necessary to take also into account intrinsic effects coming from electron reflections at perfect interfaces (a consequence of band mismatch).

Most of our GMR measurements have been performed in the current perpendicular to the plane (CPP) geometry which, in a diffusive regime,[2] permits a quantitative analysis[3] of the GMR in terms of interface resistance $r_{\uparrow(\downarrow)}=2[1 \mp \gamma]r_b^*$ and bulk resistivities $\rho_{\uparrow(\downarrow)}=2[1\mp\beta]\rho_F^*$ and $\rho_{\uparrow(\downarrow)}=2\rho_N^*$ in ferromagnetic ($F$) and nonmagnetic ($N$) layers, respectively. In these expressions $\beta$ and $\gamma$ are the spin asymmetry coefficients from bulk and interface scattering respectively. Most of our samples are multilayers in which two different metals or alloys are alternating in successive ferromagnetic layers; the GMR is then a first order function of $\beta$ and $\gamma$ in each type of ferromagnetic layer, which allows us to determine not only the magnitude but also the sign of these coefficients.[4,5] We find that both of them can be positive or negative, and that their sign can be related to characteristic features of the electronic structure.[6,7] Opposite signs of the interface and bulk coefficients give rise to a compensation thickness at which the GMR is zero. Opposite signs in consecutive $F$ layers give rise to inverse GMR. We have also performed current in plane (CIP)-GMR measurements on the same samples and we compare results obtained in the two geometries. We show how the difference can be explained by the different role of the multilayer intrinsic potential in CIP and CPP.

In Sec. II, we present pending questions in the understanding of the GMR. Section III is a note on the inverse GMR and its usefulness in determining the sign of the spin asymmetry coefficients. In Sec. IV, we describe the preparation and structural characterization of the samples. We present magnetization and CPP-GMR measurements in doped multilayers in Sec. V, and the analysis of the CPP-GMR data and the determination of the bulk spin asymmetry coefficient $\beta$ in Sec. VI. Our results on $\beta$ are discussed in Sec. VII. In Sec. VIII, we present CPP-GMR measurements from which the interface spin asymmetry coefficient $\gamma$ can be determined for several interfaces and we discuss the sign of $\gamma$. In Sec. IX, we explain why inverse GMR can only be relatively small. In Sec. X, we compare our CIP and CPP results on the same samples, and we discuss the origin of the difference between the two geometries. Section IX summarizes the results of our work and conclusions drawn from it.

## II. OPEN QUESTIONS FOR THE UNDERSTANDING OF GMR

Before presenting our work, we want to summarize the current understanding of GMR and list the questions which are still open. From a quantum mechanical point of view, the problem posed by the GMR is that of the propagation of electrons in the potential landscape represented schematically in Fig. 1 for simple $\cdots/F/N/F/N/\cdots$ multilayers in

 ©1999 The American Physical Society

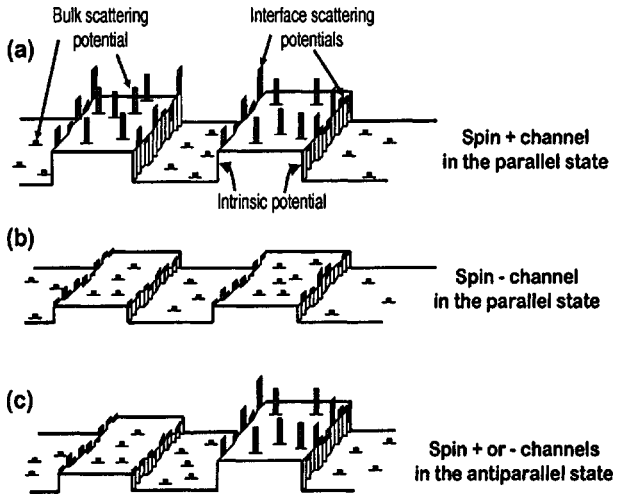


FIG. 1. Potential landscape seen by spin+ and spin− conduction electrons in the parallel and antiparallel configurations. The intrinsic potential is represented by a periodic array of barriers (Kronig-Penney-like potential); the extrinsic bulk and interface scattering potentials are represented by spikes.

which $\beta$ and $\gamma$ have the same sign. The potential seen by electrons includes the intrinsic potential of the multilayered structure and the extrinsic scattering potentials due to defects.

(i) The intrinsic potential is the potential of the perfect structure. It is periodic for periodic multilayers; its period is equal to the chemical period of the multilayer for the parallel ($P$) configuration [Figs. 1(a) and 1(b)] and twice the chemical period for the antiparallel (AP) configuration [Fig. 1(c)]. In Fig. 1, the intrinsic potential is represented by a Kronig-Penney potential. The exchange splitting of band structures in the ferromagnetic layer is depicted by different step heights of the Kronig-Penney potential in the spin + [Fig. 1(a)] and spin− [Fig. 1(b)] channels in the $P$ configuration. In the AP configuration [Fig. 1(c)], low and high steps alternate.

(ii) The scattering potentials are random extrinsic potentials associated with defects (impurities, interface roughness) and are represented by spikes in Fig. 1. In a first approximation, the interface scattering potentials can be viewed as an excess or deficit potential due to some modulation of the steps by roughness. They are obviously spin dependent since the steps are at the interfaces between magnetic and nonmagnetic metals. The scattering potentials of impurities and defects within the magnetic layers are also spin dependent, as it is well known from experiments on bulk materials.[8]

Both the intrinsic potential (steps in Fig. 1) and the scattering potentials (spikes in Fig. 1) generate GMR in CIP as well as in CPP geometry. The GMR generated by spin dependent scattering has been taken into account in the earliest models[9,10] and can be described very simply. For example, it is clear that, with the small scattering potentials in the spin+ channel of Fig. 1(b), there will be a short circuit effect by this channel with weak scattering and therefore a smaller resistivity in the $P$ configuration. On the other hand, the GMR generated by the intrinsic potential can be viewed in two different ways.

In a *superlattice approach*, valid when the mean free path (MFP) is much larger than the period of the multilayer, the periodic intrinsic potential determines the superlattice Bloch functions; these Bloch functions, as well as the corresponding spin + and spin − Fermi surfaces and Fermi velocities, are different for the $P$ configuration [intrinsic potential of Figs. 1(a),1(b)] and the AP configuration [intrinsic potential of Fig. 1(c)]. This gives rise to GMR effects even with only spin *independent* scattering. When, as in most experimental situations, the MFP is not much larger than the period, the relevant approach is the *layer by layer* one in which the contribution from the intrinsic potential to the GMR is described in terms of specular reflections of the electrons at an interface without interference between the specular reflections at successive interfaces. In the CPP geometry, the layer by layer approach leads to the particularly simple results that the contribution of the intrinsic potential to the GMR can be expressed by introducing spin dependent interface resistances;[11] more precisely, the interface resistance of the CPP geometry $r_{\uparrow(\downarrow)}$ includes contributions from both the intrinsic potential (interface steps in Fig. 1) and the interface extrinsic potentials giving rise to diffuse scattering (interface spikes in Fig. 1). The existence of interfaces resistances in CPP is one of the bases of the Valet-Fert (VF) model[3] which expresses the CPP-GMR as a function of the resistivity of the nonmagnetic layers $\rho_N^*$, the spin dependent resistivity of the ferromagnetic layers $\rho_{\uparrow(\downarrow)}=2[1\mp\beta]\rho_F^*$, the interface resistances $r_{\uparrow(\downarrow)}=2[1\mp\gamma]r_b^*$, and the spin diffusion length (SDL) in the nonmagnetic and ferromagnetic layers, $l_{sf}^N$ and $l_{sf}^F$, respectively. In the long SDL limit, when the thicknesses are smaller than the SDL, the general expressions of the VF model are reduced to the simple ones of the resistor series model that has been introduced and probed by extensive measurements at Michigan State University.[12,13]

The open questions concerning the origin of the GMR are the following.

(1) Is the GMR mainly an *extrinsic* effect resulting from spin dependent scattering by imperfections and impurities, or is it due to the *intrinsic* potential of the multilayers without any need of spin dependent scattering? *Spin dependent scattering within the ferromagnetic layers* appears via the bulk parameters $\rho_F^*$ and $\beta$; we report here that a few percent of impurities can strongly influence and even change the sign of the GMR, which demonstrates the importance of this bulk extrinsic contribution. On the other hand, the contributions from the *intrinsic potential* and the *interface extrinsic potentials* are both contained in the interface parameters $r_b^*$ and $\gamma$. We derive these parameters for a number of interfaces. However, the separation between the intrinsic and extrinsic contribution to the interface resistance is not really in the scope of this paper. In other words, our experiments allow us to separate easily the bulk extrinsic contribution from the interface resistance, but a clear identification of the intrinsic and extrinsic contributions to the interface parameters would require additional measurements on samples in which the interface imperfections can be controlled.

(2) Can the spin asymmetry coefficients $\beta$ and $\gamma$ be interpreted by electronic structure arguments? Are the coefficients $\beta$ derived from GMR in agreement with those found in bulk dilute alloys[8,15] or derived from numerical electronic structure calculations?[6,7] Since positive and negative spin asymmetries have been derived in bulk materials, can posi-

tive and negative values for $\beta$ and $\gamma$ also be found in multilayers? Is there some similarity between the coefficient $\beta$ of a $FN$ alloy and the coefficient $\gamma$ of the $F/N$ interface? We will see that our experiments allow us to give a positive answer to all these questions and, in particular, to derive coefficients $\beta$ and $\gamma$ of both signs.

(3) Can the difference between CIP and CPP measurements be clearly explained? Of course, it is already well known that the scaling lengths governing the thickness dependence are the MFP in CIP and the much larger SDL in CPP, and this explains a large part of the difference for thick layers.[3] But the difference between the scaling lengths does not count when the thicknesses are much smaller than both the MFP and SDL, whereas, even in this thin layer limit, the CPP-GMR is still generally larger than the CIP-GMR. Moreover, in the experiments we present in this article, the GMR can be inverse in the CPP geometry and normal in CIP. On the theoretical side, the models with only spin dependent scattering of free electrons (i.e., without intrinsic potential) predict the same GMR in the thin layer limit for both geometries, but a difference is expected when the intrinsic potential is introduced.[16] As it will be discussed in Sec. X, this difference likely results from the different role of the intrinsic potential in the two geometries: in CPP it introduces interface resistance, whereas it influences the GMR by channeling effects in CIP.

## III. NOTE ON INVERSE GMR

Inverse GMR (Refs. 17,18,5) can be obtained when magnetic layers $F1$ and $F2$ with opposite spin asymmetries are alternating in $[F1/N/F2/N]\times n$ structures. Suppose that the electrons propagating more easily are, for example, the minority spin electrons in $F1$ and the majority spin electrons in $F2$; then, in the antiparallel magnetic configuration, there is a short circuit effect by the channel of electrons which are minority spin electrons in $F1$ and majority spin electrons in $F2$. This means smaller resistance in the antiparallel configuration or, in other words, inverse GMR. Inverse GMR of this type has been observed in CIP by George *et al.*[17] and Renard *et al.*,[18] and in CPP by Hsu *et al.*[4] and Vouille *et al.*[5]

In the CPP geometry, the conditions for inverse GMR can be described more quantitatively in terms of the bulk and interface spin asymmetry coefficients, $\beta$ and $\gamma$. A general situation we have encountered in our samples is $\beta_1<0$ in $F1$ and $\gamma_1>0$ at the $F1/N$ interface and $\beta_2>0$ in $F2$ and $\gamma_2>0$ at the $F2/N$ interface. In this situation, an inverse GMR is expected when the global spin asymmetry of $F1$ is negative, that is when, for thick enough $F1$ layers, the bulk contribution is predominant in $F1$. Quantitatively, in the conventional resistor series model corresponding to the long SDL limit of the Valet-Fert model, a layer $F1$ introduces resistances $[1\mp\beta_1]\rho^*_{F1}t_{F1}$ and $2[1\mp\gamma_1]r^*_b$ in the spin $+$ (spin $-$) channel and the conditions for a spin independent total resistance is

$$\beta_1\rho^*_{F1}t_{F1}+2\gamma_1 r^*_b=0 \tag{1}$$

or

$$t_{F1}=t^*=-\frac{2\gamma_1 r^*_b}{\beta_1\rho^*_{F1}}. \tag{2}$$

$t^*$ is the compensation thickness at which the GMR is zero, with normal GMR for $t_{F1}<t^*$ and inverse GMR for $t_{F1}>t^*$, as for example in the measurements of Hsu *et al.*[4] and Vouille *et al.*[5] The existence of a compensation thickness with zero GMR is the signature of opposite signs of $\beta_1$ and $\gamma_1$; the inversion for $t_{F1}>t^*$ means that if $\beta_2$ and $\gamma_2$ are known to be positive, $\beta_1$ is negative. This situation will be encountered below for ($F1$/Cu/Co/Cu) multilayers with $F1=Fe$Cr, $Fe$V, $Co$Cr, $Ni$Cr.

Another situation found in our experiments is that with $\beta_1>0$, $\gamma_1<0$ and a positive spin asymmetry in $F2$. In this case, Eq. (2) still gives the compensation condition for zero GMR but now, the GMR is inverse for $t_{F1}<t^*$, that is when the interface contribution with a negative $\gamma_1$ is predominant in $F1$ and normal for $t_{F1}>t^*$.

It thus turns out that the observation of inverse GMR in ($F1/N/F2/N$) multilayers can be of great interest to determine the sign of the bulk and interface spin asymmetry coefficients and also to compare directly the bulk and interface contributions when, with competing bulk and interface spin asymmetries, there is a compensation thickness. It is without saying that, to determine absolute signs, it is necessary to start the experiments on ($F1/N/F2/N$) with metals $F2$ and $N$ for which one knows the sign of $\beta_2$ in $F2$ and $\gamma_2$ for the $F2/N$ interface. As all the calculations predict a positive $\beta$ for Co and a positive $\gamma$ for Co/Cu interfaces,[19,20] we have chosen Co for $F2$ and Cu for $N$ in our first series of samples.

## IV. PREPARATION, CHEMICAL AND STRUCTURAL CHARACTERIZATION OF THE MULTILAYERS, EXPERIMENTAL TECHNIQUES

Multilayers were deposited on silicon (001) substrates by sputtering in a ultrahigh vacuum compatible four targets system at Michigan State University using preparation conditions and procedure described elsewhere.[21,22] The CPP measurements are made on a central portion of the multilayer sandwiched between a pair of crossed Nb strips (one below, the other above). Two narrower strips of the multilayer bring the CIP current into and out of the central region. Details regarding the geometry and fabrication of the samples, including the *in situ* mask changing system are discussed at length in previous publications.[22,23] The layers of $Co_{91}Fe_9$ and $Ni_{84}Fe_{16}$ (permalloy or Py) were deposited from alloy targets. For alloys such as $Fe$Cr, $Fe$V, $Co$Cr, $Co$Mn, $Ni$Cr, $Ni$Cu with concentrations from 2.5–30 % the deposition was performed from Fe, Co, or Ni targets in which small plugs of the second element were inserted.

The chemical composition of the deposited layers, especially for the alloys, was determined by energy dispersive spectroscopy (EDS), and the concentrations indicated in the paper are those derived from these measurements. The homogeneity of the samples was also checked by the same technique.

Structural characterizations by low angle and high angle x-ray measurements confirmed the strongly (111) textured structure already observed in previous samples obtained under the same growth conditions at Michigan State University.

The periods derived from the low angle data also confirmed the nominal thicknesses of our samples. Transmission electron microscopy performed on a similar structure (NiFe/Ag/Co/Ag) (Ref. 14) showed the high quality of the superstructure for a thickness of few periods with a wavy layering afterwards. In order to check that the magnetoresistance behavior we observed in our samples is not related to a structural transition by doping, we performed x-ray-absorption-near-edge-structure (XANES) experiments at the Fe $K$ edges on FeV/Cu/Co/Cu multilayers and FeV thin films. As references for XANES, we also measured bulk Fe bcc and bulk Cu fcc. Our results for various thicknesses of alloy showed no change in the bcc structure of Fe.

The magnetization measurements have been done with a SQUID magnetometer. A reference resistor and SQUID-based null detector were used to measure the CPP magnetoresistance. At the measuring temperature of 4.2 K, the Nb strips are superconducting, becoming equipotential contacts and thereby ensuring that a uniform current passes through the overlap area $A$ ($A \sim 1.25$ mm$^2$) between the strips. In the CPP geometry, we measure $AR$, the product of the area $A$ and the resistance of the multilayer. $A$ was measured by a Dektak profilometer. Further details have been provided in an earlier publication.[12,22] A field is applied in the plane of the layers which is also an easy plane for the magnetization. In the CPP geometry, the magnetization therefore remains perpendicular to the current. Under these conditions, there is no contribution from anisotropic magnetoresistance (AMR) to the measurements.

## V. INVERSE CPP-GMR DUE TO NEGATIVE $\beta$ IN DOPED MULTILAYERS

We have studied the magnetoresistance of multilayers series of the type

$$[F1(t)/\mathrm{Cu}(4\ \mathrm{nm})/\mathrm{Co}(0.4\ \mathrm{nm})/\mathrm{Cu}(4\ \mathrm{nm})]\times 20, \quad (3)$$

where $F1$ is an alloy, $F1 = Fe\mathrm{Cr}$, $Fe\mathrm{V}$, $Co\mathrm{Cr}$, $Co\mathrm{Cr}$, $Co\mathrm{Mn}$, $Ni\mathrm{Cr}$, $Ni\mathrm{Cu}$ with concentrations of V, Cr, Mn, or Cu ranging from 2.5 to 30%. The thickness of the $F1$ layer varies generally between 1 and 7 nm. The relatively large thickness of the Cu layers, 4 nm, was chosen to prevent exchange interactions between the magnetic layers. The very small nominal thickness of the Co layers, 0.4 nm, is chosen to obtain a high coercive field for these layers, and thus a field range of antiparallel configuration between the small coercive field of the layer $F1$, typically $10^2$ Oe, and the large coercive field of the Co layers. One indeed knows from previous measurements[24] that, with 0.4 nm of Co deposited under the same conditions, the layer is discontinuous and exhibits hard magnetic properties at low temperature. After saturation in, say, the positive direction, its remanent magnetization remains almost equal to the saturation magnetization value down to negative fields of about 100–200 Oe and a field as large as 2–3 kOe is required to reverse the magnetization and saturate it in the negative direction.[24]

In Fig. 2(a), we show a typical example of magnetization curve, obtained for $[Fe\mathrm{Cr}\ 30\%\ (8.5\ \mathrm{nm})/\mathrm{Cu}(4\ \mathrm{nm})/\mathrm{Co}(0.4\ \mathrm{nm})/\mathrm{Cu}(4\ \mathrm{nm})]\times 20$. A two step reversal is clearly seen: the abrupt reversal at about zero field (at the scale of the figure) is that of the $Fe\mathrm{Cr}$ layers. The second step saturating at about 2 kOe is that of the ultrathin Co layers. In Fig. 2, we can compare the magnetization and MR curves for the same sample. On the curve of (inverse) GMR, the resistance decreases abruptly when the magnetization of the $Fe\mathrm{Cr}$ layers switches at low field; then the resistance increases again slowly and reaches its initial value at about 2 kOe. The slow increase above 2 kOe is a spurious effect related to the influence of the applied field on the superconducting Nb layers and can be corrected.

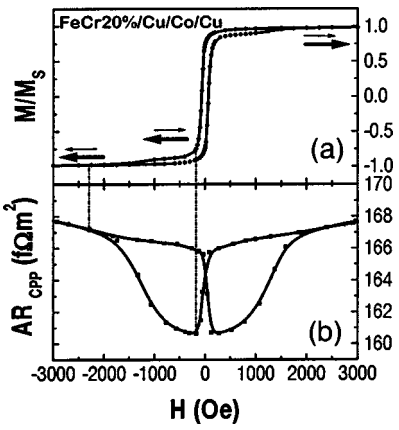


FIG. 2. Magnetization and CPP-MR curves for a $[Fe\mathrm{Cr}\ 20\%(6.5\ \mathrm{nm})/\mathrm{Cu}(4\ \mathrm{nm})/\mathrm{Co}(0.4\ \mathrm{nm})/\mathrm{Cu}(4\ \mathrm{nm})]\times 20$ multilayer. $AR_{\mathrm{CPP}}$ is the resistance normalized to unit area ($R_{\mathrm{CPP}}$ = measured resistance, $A$ = area of the sample). Arrows indicate the orientation of the magnetization in the $Fe\mathrm{Cr}$ (large arrow) and Co (thin arrow) layers at several values of the applied field.

In Fig. 3, we show the MR curves for a series of $[Ni\mathrm{Cr}\ 5\%(t)/\mathrm{Cu}(4\ \mathrm{nm})/\mathrm{Co}(0.4\ \mathrm{nm})/\mathrm{Cu}(4\ \mathrm{nm})]\times 20$

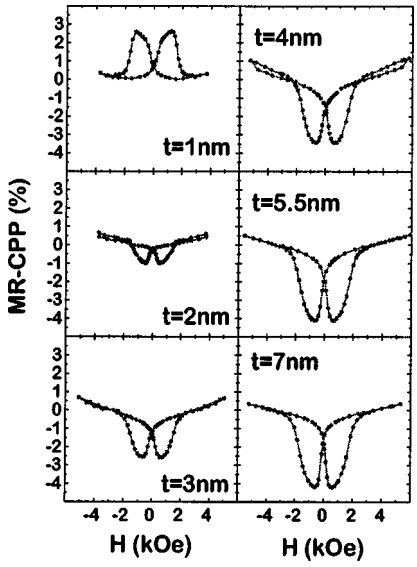


FIG. 3. CPP-MR curves for a series of $[Ni\mathrm{Cr}\ 5\%(t)/\mathrm{Cu}(4\ \mathrm{nm})/\mathrm{Co}(0.4\ \mathrm{nm})/\mathrm{Cu}(4\ \mathrm{nm})]\times 20$ multilayers with several values of the thickness $t$, as indicated on the figure. For $t \geq 2$ nm, the contribution from bulk scattering with $\beta_{\mathrm{NiCr}} < 0$ is predominant in the $Ni\mathrm{Cr}$ layers, which leads to inverse GMR. For $t = 1$ nm, the contribution from the $Ni\mathrm{Cr}/\mathrm{Cu}$ interfaces with $\gamma_{\mathrm{NiCr/Cu}} > 0$ is predominant and the GMR is normal. The thickness of compensation between negative $\beta$ and positive $\gamma$ is around 1.7 nm, see Fig. 5.

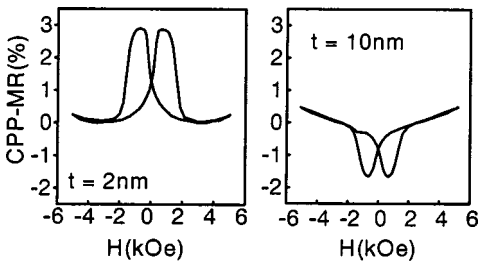


FIG. 4. Normal (left) and inverse (right) CPP-GMR curves for $[NiCr\ 2.5\%(t)/Cu(4\ nm)/Co(0.4\ nm)/Cu(4\ nm)]\times 20$ multilayers with $t_{NiCr}=2$ nm (left) and $t_{NiCr}=10$ nm (right).

multilayers with $t$ increasing from 1 to 7 nm. One sees the behavior expected in Sec. III when $\beta_1$ (i.e., $\beta_{NiCr}$) is negative, and $\gamma_1$ (i.e.; $\gamma_{NiCr/Cu}$), $\beta_2$ (i.e., $\beta_{Co}$), and $\gamma_2$ (i.e., $\gamma_{Co/Cu}$) are positive. The GMR is normal (i.e., $R_{AP}>R_P$) for $t=1$ nm when the major contribution from the $Ni$Cr layers to the GMR comes from the interface resistance; then, for $t \geqslant 2$ nm, when the bulk contribution is predominant in the $Ni$Cr layers, the GMR is inverse ($R_{AP}<R_P$). The same behavior is also observed for $Ni$Cr 2.5%, as illustrated in Fig. 4. In contrast, the GMR is always normal without Cr impurities (curves not shown here), which means that 2.5 at. % of Cr is sufficient to change the sign of $\beta$ and reverse the GMR.

In Fig. 5, we show the variation of the MR ratio as a function of the thickness $t$ of the $F1$ layers for $F1=Ni$Cr 5%, $Ni$Cu 30% and pure Ni. For $F1=Ni$Cr 5%, one sees the crossover from normal to inverse GMR as $t$ increases, the GMR is zero at $t^*=1.7$ nm, which is the compensation thickness at which the contributions from the positive interface spin asymmetry ($\gamma$) and the negative bulk spin asymmetry ($\beta$) cancel one another. In contrast, for $F1=Ni$Cu 30%, as for pure Ni, there is no inversion and the GMR is always normal; this means that in contrast with the case involving Cr impurities, Cu impurities introduce scattering centers with positive spin asymmetry, so that the sign of $\beta$ remains positive. In Figs. 6 and 7 we show the variation of

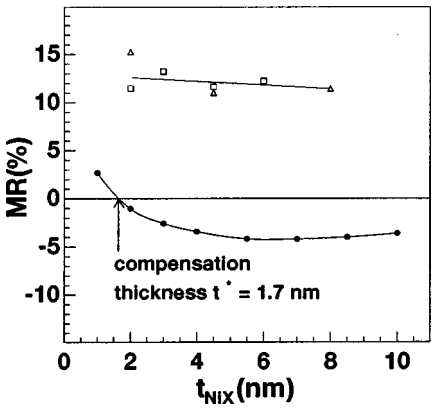


FIG. 5. Variation of the CPP-GMR ratio in $[F1(t)/Cu(4\ nm)/Co(0.4\ nm)/Cu(4\ nm)]\times 20$ multilayers as function of the thickness $t$ of layer $F1$ for $F1=Ni$Cr 5% (●), $F1=Ni$Cu 30% (△), and pure Ni (□). The figure illustrates the different behavior for $\beta_{F1}<0$ (inversion above the compensation thickness $t^*\simeq 1.7$ nm for $F1=$NiCr 5%) and $\beta_{F1}>0$ (no inversion for $F1=$NiCu 30% or pure Ni), in all cases with $\gamma_{F1/Cu}>0$, $\beta_{Co}>0$, and $\gamma_{Co/Cu}>0$.

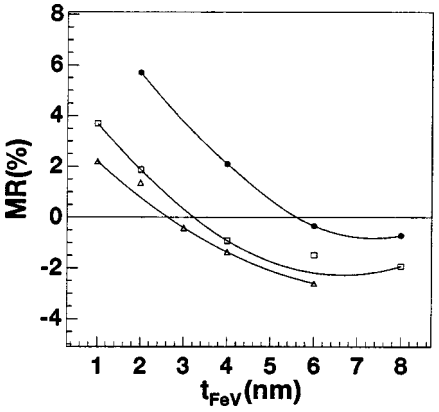


FIG. 6. Variation of the CPP-GMR ratio in $[F1(t)/Cu(4\ nm)/Co(0.4\ nm)/Cu(4\ nm)]\times 20$ multilayers as function of the thickness $t$ of the $Fe$V layers for $Fe$V 15% (●), $Fe$V 22% (□), and $Fe$V 28% (△). The compensation thickness between the contributions from positive $\gamma_{FeV/Cu}$ and negative $\beta_{FeV}$ decreases as $|\beta_{FeV}\rho^*_{FeV}|$ increases with the concentration of vanadium, as expected from Eq. (2).

the MR ratio as a function of the thickness of layer $F1$ for $F1=Fe$V 15%, $Fe$V 22%, $Fe$V 28%, $Co$Mn 5%, $Co$Mn 18%. For $Fe$V, the behavior is the same as for $Ni$Cr, with an inversion of the GMR for thicknesses of layers $F1$ above a thickness $t^*$ of compensation between a positive $\gamma$ and a negative $\beta$. For $Co$Mn, the GMR decreases rapidly with $t$ but is not reversed; we will see from the analysis of the data, that this behavior also corresponds to a negative $\beta$ but too small to compensate the positive $\gamma$ in the range of $t_{CoMn}$ in our samples.

## VI. ANALYSIS OF CPP-GMR IN DOPED MULTILAYERS AND DETERMINATION OF THE SPIN ASYMMETRY COEFFICIENTS

We have analyzed the experimental results of Sec. V with the expressions of the long SDL limit of the VF model,[3] that is, equivalently, the expressions of the series resistor model.[12,13] These expressions have already been extensively tested at Michigan State University and other laboratories.[13,25] For a structure of the type $(Nb/[F1(t_{F1})/N(t_N)/F2(t_{F2})/N(t_N)]\times n/F1(t_{F1})/Nb)$ and

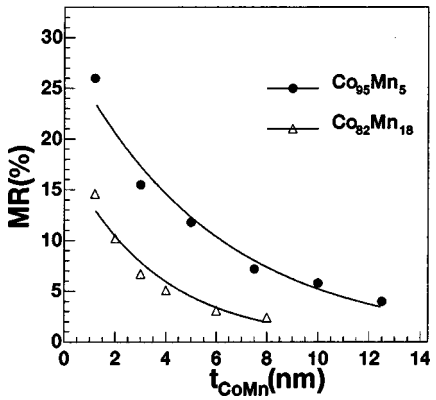


FIG. 7. Variation of the CPP-GMR ratio in $[CoMn(t)/Cu(4\ nm)/Co(0.4\ nm)/Cu(4\ nm)]\times 20$ multilayers as function of the thickness $t$ of the $Co$Mn layers and for two concentrations of Mn.

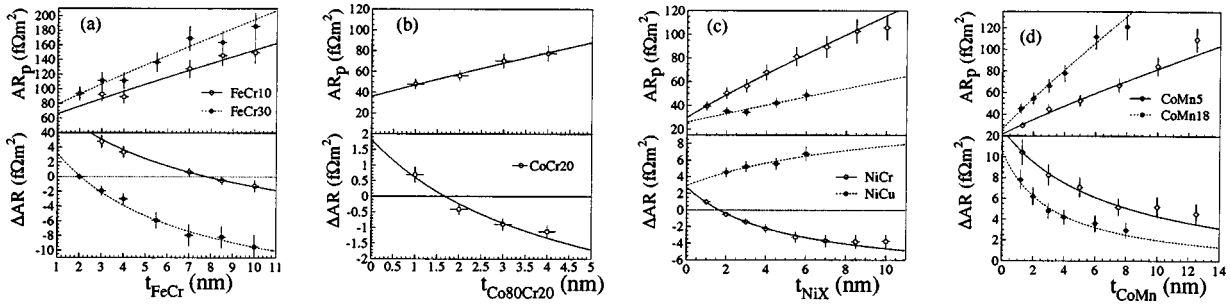


FIG. 8. Fit of the variation of normalized resistance in the parallel configuration $AR_p$, and magnetoresistance $A\Delta R = A(R_{AP} - R_P)$, as a function of the thickness $t_{F1}$ for $[F1(t)/\mathrm{Cu}(4\ \mathrm{nm})/\mathrm{Co}(0.4\ \mathrm{nm})/\mathrm{Cu}(4\ \mathrm{nm})]\times 20$ multilayers with (a) $F1 = Fe\mathrm{Cr}$ 10% and 30%, (b) $F1 = Co\mathrm{Cr}$ 20%, (c) $F1 = Ni\mathrm{Cr}$ 5% and $Ni\mathrm{Cu}$ 30%, (d) $F1 = Co\mathrm{Mn}$ 5% and 18%. The curves are calculated with the expressions of the long SDL limit of the VF model, as explained in the text. Only the experimental points corresponding to values of $t_{F1}$ which are smaller than $1.5 l_{SF}^{F_1}$ (see text for an approximate extimate of the SDL) have been taken into account for the fit.

with the notation already introduced in Sec. I to express the spin dependence of the unit area interface resistance $r_{\uparrow(\downarrow)}$ and the layer resistivities $\rho^F_{\uparrow(\downarrow)}$ and $\rho^N_{\uparrow(\downarrow)}$, the spin + and spin − resistances in the $P$ and $AP$ configurations and for a unit area can be written as

$$AR_P^{+(-)} = 4r^*_{Nb/F1} + 2n\rho^*_N + 2n[1 \mp \gamma_{F1/N}]r^*_{F1/N} + (n+1)[1 \mp \beta_{F1}]\rho^*_{F1} + 2n[1 \mp \gamma_{F2/N}]r^*_{F2/N} + n[1 \mp \beta_{F2}]\rho^*_{F2}, \quad (4)$$

$$AR_{AP}^{+(-)} = 4r^*_{Nb/F1} + 2n\rho^*_N + 2n[1 \mp \gamma_{F1/N}]r^*_{F1/N} + (n+1)[1 \mp \beta_{F1}]\rho^*_{F1} + 2n[1 \pm \gamma_{F2/N}]r^*_{F2/N} + n[1 \pm \beta_{F2}]\rho^*_{F2}, \quad (5)$$

where $r^*_{\mathrm{Nb}/F1}$ is the resistance of the Nb/$F1$ interface (independently determined).

The CPP resistances of the $P$ and $AP$ configurations, $R_P$ and $R_{AP}$, are written as

$$AR_{P(AP)} = \frac{AR^+_{P(AP)} AR^-_{P(AP)}}{AR^+_{P(AP)} + AR^-_{P(AP)}}. \quad (6)$$

The above expressions, Eqs. (4), (5), (6), hold in the long SDL limit, that is when, for each type of layer, the SDL is longer than the thickness of the layer. When the thickness exceeds the SDL, the MR is smaller than what is expected from these expressions,[3] and, typically, the deviation approaches 15% for $t_F \approx 1.5 l^F_{sf}$ and 25% for $t_F \approx 2 l^F_{sf}$.[26] The long SDL limit is largely justified for the Cu and Co layers ($t_{\mathrm{Cu}} = 4$ nm, $t_{\mathrm{Co}} = 0.4$ nm), since the SDL at low temperature has been estimated at 140 nm in Cu and 59 nm in Co.[25] The case of the $F1$ layers, with $F1 = Fe\mathrm{Cr}$, $Fe\mathrm{V}$, $Co\mathrm{Cr}$, $Co\mathrm{Cr}$, $Ni\mathrm{Cr}$, $Ni\mathrm{Cu}$ deserves a more quantitative discussion. We recall the expression of the SDL in a ferromagnetic metal or alloy:[3]

$$l^F_{sf} = \sqrt{\frac{\lambda^*_F \lambda_{sf}}{6}}, \quad (7)$$

where, in a free electron model, $\lambda^*_F = (\lambda_\uparrow^{-1} + \lambda_\downarrow^{-1})^{-1}$ is related to the resistivity $\rho^*_F$ by the classical expression

$$\lambda^*_F = \frac{\hbar k_F}{n e^2 \rho^*_F}. \quad (8)$$

The spin MFP, $\lambda_{sf} = v_F \tau_{sf}$, where $\tau_{sf}$ is the spin-lattice relaxation time, is due, at least at low temperature, to the spin-orbit part of the elastic scattering by defects or impurities.[27] According to the analysis of extensive ESR data[28] $\lambda_{sf} = s\lambda^*_F$, where $s$ is of the order of $10^2$ when the scattering is by $3d$ impurities. Consequently, for our alloys, $l^F_{sf}$ is expected to be roughly proportional to $1/\rho^*_F$. The quantitative discussion of the SDL in $Cu\mathrm{Ni}$ alloys by Hsu *et al.*[29] is based on this approach and confirms that $l^F_{sf}$ decreases progressively from 23 nm for $Cu\mathrm{Ni}$ 6.9% with $\rho^*_{Cu\mathrm{Ni}} = 11\ \mu\Omega$ cm to 7.5 nm for $Cu\mathrm{Ni}$ 22.7% with $\rho^*_{\mathrm{CuNi}} = 30.3\ \mu\Omega$ cm. The resistivity of our alloys are in the range 16.7–67 $\mu\Omega$ cm, which roughly means that the SDL range is between 13.6 and 3.3 nm. We have applied our analysis to samples with $t_F < 1.5 l^{F1}_{sf}$. An analysis with the general expressions of the VF model requires the introduction of additional free parameters (the SDL) and is less tranparent; we publish elsewhere an analysis of this type for another series of samples.[30] Here, we have performed a simpler analysis using the expressions in the long SDL limit, even if we know that this leads to a small underestimate of the spin asymmetry coefficient.

We have fitted Eqs. (4), (5), (6) with our experimental data for $AR_P$ and $A\Delta R = AR_{AP} - AR_P$ by using values of the parameters $\rho^*_{\mathrm{Cu}}$, $\beta_{\mathrm{Co}}$, $\rho^*_{\mathrm{Co}}$, $\gamma_{\mathrm{Co/Cu}}$, $r^*_{\mathrm{Co/Cu}}$, $r^*_{\mathrm{Co/Nb}}$ already derived at MSU for layers prepared in the same conditions[31] and leaving $\beta_{F1}$, $\rho^*_{F1}$, $\gamma_{F1/\mathrm{Cu}}$, $r^*_{F1/\mathrm{Cu}}$ as free parameters. The best fits obtained for the variation of $AR_P$ and $A\Delta R$ with $t_{F1}$ are shown in Fig. 8 for several series of samples of the type $[F1(t)/\mathrm{Cu}(4\ \mathrm{nm})/\mathrm{Co}(0.4\ \mathrm{nm})/\mathrm{Cu}(4\ \mathrm{nm})]\times 20$. The fits for $Fe\mathrm{V}$ have been presented in Ref. 4 and are not shown.

The parameters $\beta_{F1}$, $\rho^*_{F1}$, $\gamma_{F1/\mathrm{Cu}}$, $r^*_{F1/\mathrm{Cu}}$ giving the best fits for $F1 = Fe\mathrm{Cr}$ 10%, $Fe\mathrm{Cr}$ 30%, $Fe\mathrm{V}$ 15%, $Fe\mathrm{V}$ 22%, $Fe\mathrm{V}$ 28%, $Co\mathrm{Cr}$ 10%, $Co\mathrm{Mn}$ 5%, $Co\mathrm{Mn}$ 18%, $Ni\mathrm{Cr}$ 5%, $Ni\mathrm{Cu}$ 30% are listed in Table I; the compensation thickness $t^*$ for the samples with inverse GMR are also given in the last column. In systems exhibiting an inverse GMR, we find that, as expected, $\beta$ is negative. As also expected, we find a positive $\beta$ for $Ni\mathrm{Cu}$ (no inversion). The case of $Co\mathrm{Mn}$ is marginal. There is no inversion, but, in contrast with the case

TABLE I. Best fit parameters obtained for the interface resistance $AR^*_{F/Cu}$, resistivity $\rho^*_F$, $\gamma_{F/Cu}$, and $\beta_F$ for different ferromagnetic alloys and pure Co. The compensation thickness $t^*$ is derived from Eq. (2) with the parameters of the table.

| Alliage | $AR^*_{F/Cu}$ ($f\Omega$ m$^2$) | $\gamma_{F/Cu}$ | $\rho^*_F$ ($n\Omega$ m) | $\beta_F$ | $t^*$ (nm) |
|---|---|---|---|---|---|
| $Co_{90}Cr_{10}$ | 0.18±0.07 | 0.35±0.12 | 430±40 | −0.12±0.01 | 2.4 |
| $Co_{80}Cr_{20}$ | 0.36±0.07 | 0.08±0.03 | 450±62 | −0.08±0.03 | 1.6 |
| $Co_{95}Mn_5$ | 0.19±0.04 | 0.96±0.19 | 243±24 | −0.03±0.03 | 50 |
| $Co_{82}Cr_{18}$ | 0.26±0.07 | 0.63±0.15 | 566±48 | −0.01±0.02 | 58 |
| $Fe_{90}Cr_{10}$ | 0.75±0.15 | 0.37±0.07 | 424±47 | −0.16±0.03 | 8.2 |
| $Fe_{70}Cr_{30}$ | 0.87±0.16 | 0.21±0.05 | 597±76 | −0.28±0.04 | 2.2 |
| $Fe_{85}V_{15}$ | 0.36±0.14 | 0.58±0.08 | 542±57 | −0.11±0.04 | 5.7 |
| $Fe_{81}V_{19}$ | 0.56±0.12 | 0.30±0.06 | 644±56 | −0.11±0.03 | 4.4 |
| $Fe_{78}V_{22}$ | 0.61±0.08 | 0.22±0.03 | 672±45 | −0.12±0.02 | 3.1 |
| $Ni_{95}Cr_5$ | 0.27±0.04 | 0.15±0.03 | 373±23 | −0.13±0.01 | 1.7 |
| $Ni_{70}Cu_{30}$ | 0.19±0.04 | 0.21±0.06 | 167±30 | +0.19±0.04 | |
| $Ni_{79}Fe_{21}$ (Ref. 33) | 0.5 | 0.76 | 220 | +0.65 | |
| $Co_{91}Fe_9$ (Ref. 32) | 0.52 | 0.76 | 70 | +0.65 | |
| Co (Ref. 31) | 0.525 | 0.75 | 76 | +0.46 | |

of *Ni*Cu for which $\Delta R$ increases with $t_{NiCu}$, $\Delta R$ decreases rapidly as a function of $t_{CoMn}$. This suggests that $\beta_{CoMn}$ is negative but too small to compensate the contribution from the positive $\gamma_{CoMn/Cu}$ in the experimental range of $t_{CoMn}$. This is confirmed by the calculation which finds that the best fit is obtained for a negative but very small value of $\beta_{CoMn}$ $(-0.03)$.

The negative contribution to $\beta$ induced by Cr or V impurities competes with the positive contribution from structural defects, so one expects that a minimum concentration is required to invert $\beta$ and the GMR. For *Ni*Cr, 2.5% of Cr is sufficient to invert the GMR. For *Fe*V, one sees in Fig. 9 that $\beta_{FeV}$ is stabilized to an approximatively constant negative value between 15 and 28%; this means that, in this concentration range, the contribution from scattering by V impurities is already predominant and determines $\beta_{FeV}$. For *Co*Cr, $\beta$ is also roughly constant in our 10–20% concentration range but for *Fe*Cr, $\beta$ does not seem to be stabilized at 10% and varies from $-0.16$ at 10% to $-0.28$ at 30%. We also see in Fig. 9 that $\gamma_{FeV/Cu}$ decreases with the concentration of V but remains positive. This shows that, for the interface resistance, the contribution from the intrinsic potential and roughness is still larger than the impurity contribution at concentrations as high as 28%. It is straightforward to check that, with FeV layers, the decrease of the compensation thickness as the concentration of V increases is due to both the increase of $|\beta_{FeV}\rho^*_{FeV}|$ and decrease of $\gamma_{FeV/Cu}r^*_{FeV/Cu}$.

In conclusion, the results on doped multilayers presented in this section bring to the fore the importance of the extrinsic contributions to the GMR. The contribution from impurities appears in the bulk spin asymmetry $\beta$. This coefficient can be positive or negative, depending on the choice of impurity. The GMR is zero at a compensation thickness $t^*$ when, for $\beta<0$ and $\gamma>0$ in the same layer, there is competition between the bulk and interface spin asymmetries.

## VII. INTERPRETATION OF THE BULK SPIN ASYMMETRY COEFFICIENT $\beta$ IN LAYERS OF FERROMAGNETIC METAL OR ALLOY

In Fig. 10 we compare values of the spin asymmetry coefficient $\beta$ derived from CPP-GMR measurements and found

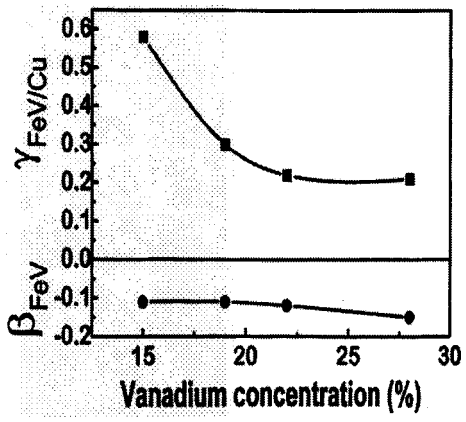


FIG. 9. Variation of the bulk and interface spin asymmetry coefficients $\beta_{FeV}$ and $\gamma_{FeV/Cu}$ as a function of the concentration of vanadium in *Fe*V layers.

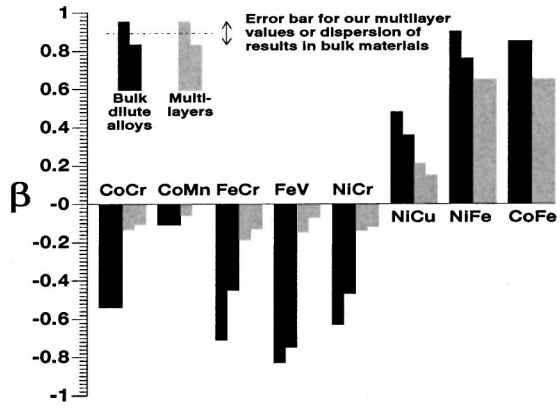


FIG. 10. Comparison of the spin asymmetry coefficients $\beta$ derived from our analysis of CPP-GMR in multilayers and found in bulk dilute alloys (Refs. 8,15).

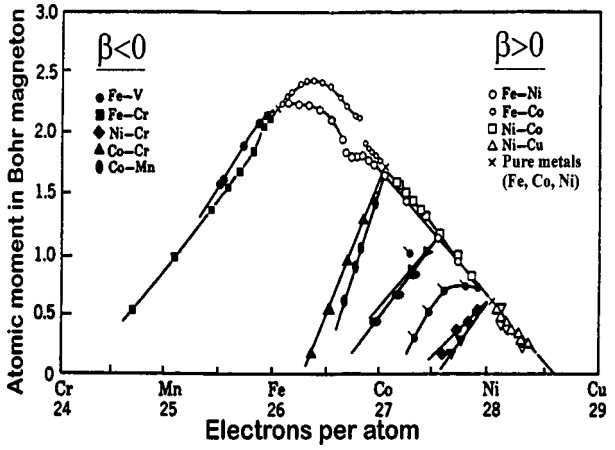


FIG. 11. Slater-Pauling plot for alloys of $3d$ metals and scattering spin asymmetry: the spin asymmetry coefficient $\beta$ is positive for the pure metals, Fe, Co, and Ni and their alloys located on the slope at $-45°$, i.e., NiCu, NiFe, CoFe; $\beta$ is negative on the branches at roughly $+45°$, i.e., for FeV, FeCr, CoCr, CoMn, and NiCr alloys.

in bulk materials.[8] We have added to the results of the present work, data derived from GMR for $Ni$Fe (permalloy) and $Co$Fe 9% in previous publications.[33,32] As we can see (i) There is a perfect agreement between multilayers and bulk alloys for the *sign* of $\beta$. The sign also agrees with what is predicted by *ab initio* calculations in dilute alloys.[6] (ii) The magnitude of $\beta$ is always smaller for the data derived from GMR measurements, however, the variation of $\beta$ throughout the alloy series of Fig. 10 is very similar for multilayers and bulk alloys. The difference between the magnitude of $\beta$ in multilayers and bulk materials is due to various effects that are discussed at the end of this section. For the moment, we want to discuss the interpretation of the sign of $\beta$ in terms of electronic structure. The physics involved appears clearly when, in Fig. 11, one looks at the different location of positive and negative $\beta$ on the classical Slater-Pauling plot for transition metals alloys. Positive values of $\beta$ are obtained for pure metals and alloys located on the regions of negative slope of the Slater-Pauling curve. Negative values of $\beta$ are found for alloys on the branches of positive slope from Fe ($Fe$Cr, $Fe$V), Co ($Co$Cr, $Co$Mn), and Ni ($Ni$Cr). This can be explained by electronic structure arguments.[6–8] The positive values of $\beta$ are associated with a higher density of states (DOS) at the Fermi level for the minority spin direction in the pure metals and on the impurity sites. In contrast, for Cr or V impurities in Fe or Cr impurities in Co or Ni, the *d* levels of the impurity are well above the host *d* band for the majority spin direction; therefore they cannot hybridize with the majority spin *d* band states. The resonant scattering of spin $\uparrow$ *s-p* electrons with empty *d* states of the impurity just above the Fermi level explains the large spin $\uparrow$ resistivity and the resulting negative sign of $\beta$; alternatively one can say that the formation of a virtual bound state leads to a high spin $\uparrow$ DOS at the Fermi level on the impurity site.

The clearly different electronic structure of alloys with positive and negative $\beta$ can be seen in the results of the *ab initio* calculations by Mertig *et al.*[6] for series of Ni, Co, and Fe based dilute alloys. In Ni with Co or Fe impurities for example, the DOS on the impurity sites looks similar to that of pure Ni, with a much higher DOS at $E_f$ in the minority spin direction and, consistently, a positive value of $\beta$ is calculated. In contrast, for example in Co with Cr or Mn impurities, the spin $\uparrow$ DOS on the impurity site presents a peak just above the Fermi level; this peak reflects the resonant scattering of the spin electrons on the impurity *d* levels in the majority spin direction and the formation of a virtual bound state.

We finally discuss the origin of the difference between the magnitude of $\beta$ in multilayers and bulk materials. First, it must be recognized that, in doped multilayers, the electrons are not only scattered by impurities but also by structural defects more concentrated than in bulk materials. As the spin asymmetry of the scattering by structural defects in Ni, Co, or Fe is positive, there is always some reduction of the negative spin asymmetry by the positive spin asymmetry of the structural defects. This probably explains a part of the discrepancy between multilayers and bulk alloys. In addition, as we have discussed above, we use the simple expressions of the long SDL limit to analyze our experimental data and this leads to some underestimate of $\beta$. A much better agreement is obtained when, in multilayers with thicker $Ni$Cr layer, the SDL can be determined and taken into account in the determination of $\beta$.[30] Finally we point out that a departure from a perfect $AP$ ordering can have a more important consequence in ($F1/N/F2/N$) structures with inverse GMR; this is because an imperfect $AP$ ordering between $F1$ and $F2$ implies that the magnetization of successive $F2$ layers is not perfectly parallel and this can add an additional normal GMR term. All the above described effects probably contribute to the difference between the values of $\beta$ in multilayers and bulk materials.

## VIII. INVERSE CPP-GMR DUE TO NEGATIVE $\gamma$

In Sec. V, we presented inverse CPP-GMR results due to the negative sign of $\beta_{F1}$ in ($F1$/Cu/$F2$/Cu) multilayers in which $\beta_{F2}$ and $\gamma_{F2/Cu}$ are positive. Here we report on inverse GMR effects due to the negative sign of $\gamma_{F1}$ in ($F1$/Cr/$F2$/Cr) multilayers in which the spin asymmetry of $F2$ is dominated by $\beta_{F2}$ and is positive.

We first present results on (Co/Cr/Py/Cr) multilayers (Py =permalloy) in which the thickness of Cr has been chosen in the first thickness range of antiferromagnetic (AF) coupling (first peak). Typical magnetization and MR curves are presented in Fig. 12. The magnetization curve reflects the AF ordering between the Co and Py layers below about 4 kOe; starting from the right of the figure, the first drop of magnetization between approximately 4 and 2 kOe is due to the reversal of the small magnetic moment of the Co layers induced by AF coupling. Then the abrupt drop at very small negative field indicates the reversal of the AF coupled Co-Py system as a whole. Finally, between about $-2$ and $-4$ kOe, the applied field overcomes the AF coupling and, by aligning the moment of Co with that of Py, saturates the magnetization in the negative direction. The (inverse) GMR curve reflects the relative orientation of Py and Co. In decreasing field, the resistance drops with the onset of an AP configuration between 4 and 2 kOe, does not vary when the AP coupled Co-Py system rotates as a whole (note the flat bot-

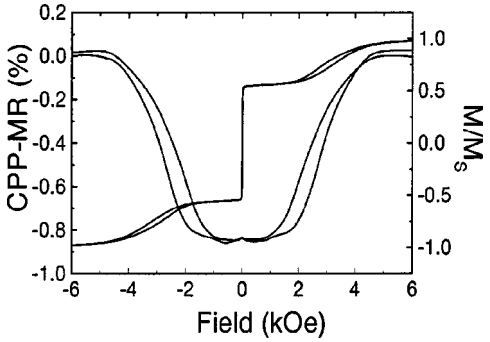


FIG. 12. Magnetization and CPP-GMR curves for a [Co(1 nm)/Cr(0.9 nm)/Py(4 nm)/Cr(0.9 nm)]×20 multilayers.

tom of the GMR curve) and comes back to its initial value between −2 and −4 kOe.

We have measured the MR of series of AF coupled (Co/Cr/Py/Cr)×$N$ samples with thick layers of Py (8 nm) as a function of the thickness of Co. As illustrated by Fig. 13, the GMR is inverse for thin Co layers and becomes normal for Co layers thicker than $t^*=6$ nm. The inverse GMR for $t_{Co}<t^*$ can be ascribed to a negative value of the interface spin asymmetry coefficient $\gamma_{Co/Cr}$ (with a global spin asymmetry dominated by $\beta_{Py}$ and positive for the Py layers); at $t_{Co}=t^*$ there is a compensation between positive $\beta_{Co}$ and negative $\gamma_{Co/Cr}$, and for $t_{Co}>t^*$, the contribution from $\beta_{Co}$ becomes predominant and the GMR is normal. The negative sign for $\gamma_{Co/Cr}$ is in agreement with theoretical calculations.[34,35]

The experimental results obtained for the Co($t$)/Cr(1.1 nm)/Py(8 nm)/Cr(1.1 nm) and $Co$Fe($t$)/Cr(0.9 nm)/$Co$Fe(4 nm)/Cr(0.9 nm) series have been fitted with the expressions of the long SDL limit of the VF model, as already explained in Sec. VI for other series of samples. We have used the parameters $\rho^*_{Co}$, $\rho^*_{Py}$, $\beta_{Py}$, $\beta_{Co}$, $\beta_{CoFe}$ already derived at MSU on samples prepared in the same conditions[31,32] and taken $\rho^*_{Cr}$, $\rho^*_{CoFe}$ and the interface parameters as free parameters. Examples of fits are shown in Fig.

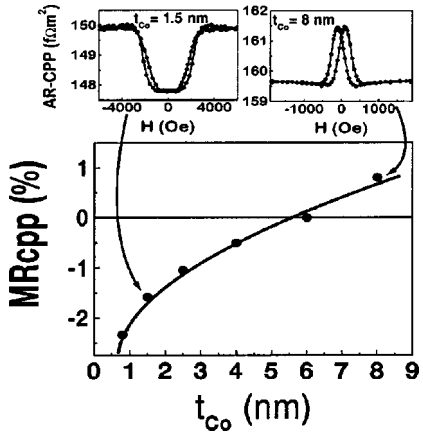


FIG. 13. Top: inverse and normal CPP-GMR curves for [Co($t$)/Cr(1.1 nm)/Py(8 nm)/Cr(1.1 nm)]×20 multilayers with $t_{Co}=1.5$ nm and $t_{Co}=8$ nm. Below, we show the variation of the MR ratio as a function of the thickness of the Co layers. The compensation thickness between negative $\gamma_{Co/Cr}$ and positive $\beta$ is about 6 nm.

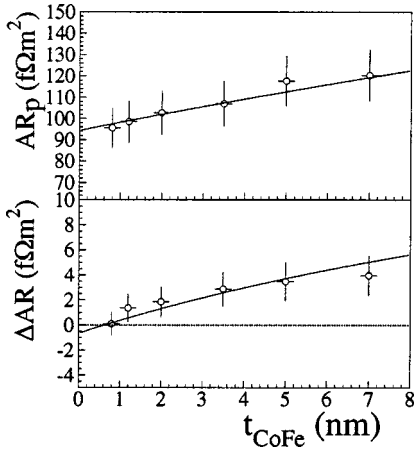


FIG. 14. Fits of the variation of the normalized resistance in the parallel configuration $AR_P$ and magnetoresistance $A\Delta R=A(R_{AP}-R_P)$, as a function of the thickness $t_{F1}$ for [$Co$Fe 10%($t$)/Cr(1.1 nm)/$Co$Fe 10%(4 nm)/Cr(1.1 nm)]×20 multilayers. The curves are calculated with the expressions of the long SDL limit of the VF model as explained in the text.

14. The best fit parameters are listed in Table II, with, as expected from the existence of inverse GMR at small values of $t$, negative values of $\gamma_{Co/Cr}$ and $\gamma_{CoFe/Cr}$. Note also that the best fit is obtained with a small negative value for $\gamma_{Py/Cr}$.

We have also prepared series of samples Fe($t$)/Cr/Py/Cr but, as the field required to overcome the AF coupling at the first peak is too strong to saturate the magnetization in the field range required to keep the Nb layers in superconducting state, we prepared samples at the second peak of AF coupling, that is for $t_{Cr}=2.4$ nm. Our results, see Fig. 15, reveal an inverse GMR for $t<4$ nm and therefore indicate that $\gamma_{Fe/Cr}$, similar to $\gamma_{Co/Cr}$, is negative. However, due probably to the high resistance of the Cr layers, and to the resulting short SDL, the MR in Fe($t$)/Cr(2.4 nm)/Py(8 nm)/Cr(2.4 nm) samples is very small. Also, since a short SDL is expected, a simple analysis with the simple expressions of Sec. VI would be an unrealistic way to determine the magnitude of the negative $\gamma_{Fe/Cr}$.

The last result we present on structures with Cr layers is that obtained on ($Fe$Cr 30%/Cr/Py/Cr) multilayers. We first want to point out that, for all the samples ($F1/N/F2/N$) with inverse GMR discussed so far in this paper, there was none with a negative sign for *both* $\beta_{F1}$ and $\gamma_{F1}$. We thus generally observe a compensation thickness $t^*$ with zero GMR and a partial compensation below and above $t^*$. This partial compensation contributes to the smallness of the inverse GMR, as discussed in the following section. We now present some results on [$Fe$Cr 30%($t$)/Cr(1.1 nm)/Py(8 nm)/

TABLE II. Best fit parameters obtained for the interface resistance $AR^*_{F/Cr}$ and $\gamma_{F/Cr}$ for Co/Cr, CoFe/Cr, and NiFe/Cr interfaces. The compensation thickness $t^*$ is derived from Eq. (2).

| Interface | $\gamma_{F/Cr}$ | $AR^*$ ($f\Omega$ m$^2$) | $t^*$ (nm) |
|---|---|---|---|
| Co/Cr | $-0.24\pm0.17$ | $0.48\pm0.13$ | 6.6 |
| CoFe/Cr | $-0.14\pm0.03$ | $0.32\pm0.05$ | 0.6 |
| NiFe/Cr | $-0.03\pm0.03$ | $0.95\pm0.17$ | |

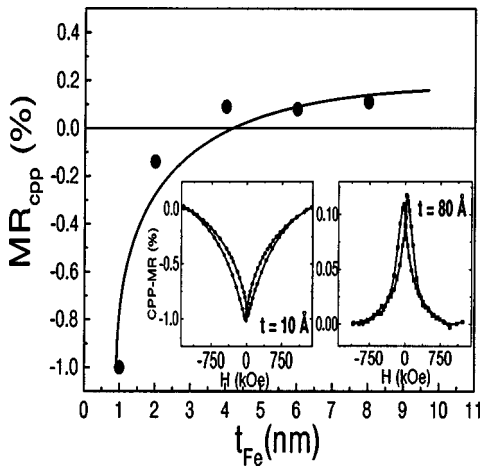


FIG. 15. Variation of the CPP-GMR ratio in [Fe($t$)/Cr(2.4 nm)/Py(8 nm)/Cr(2.4 nm)]×20 multilayers as a function of the thickness $t_{Fe}$ of the Fe layers. The compensation thickness between negative $\gamma_{Fe/Cr}$ and positive $\beta_{Fe}$ is around 4 nm.

Cr(1.1 nm)]×20 multilayers where both $\beta_{FeCr}$ and $\gamma_{FeCr/Cr}$ are negative for the $Fe$Cr layers. As this has been discussed above, the saturation field resulting from the strong AF coupling between Fe or $Fe$Cr and Py layers is too high for measurements with superconducting Nb contacts when the Fe or $Fe$Cr are thin, but, nevertheless, we could measure the GMR for $Fe$Cr layers thicker than 3 nm. In Fig. 16, we show an example of result. We can see that, with now the same sign for $\beta_{FeCr}$ and $\gamma_{FeCr/Cr}$ and no competition between opposite bulk and interface spin asymmetries in the $Fe$Cr layers, the inverse GMR can reach 15% (in spite of some remaining competition between positive $\beta_{Py}$ and negative $\gamma_{Py/Cr}$ in the Py layer).

To sum up Sec. VIII, we have found that the interface spin asymmetry coefficient $\gamma$ is negative for Co/Cr, $Co$Fe 10%/Cr, Py/Cr, Fe/Cr, and $Fe$Cr 30%/Cr interfaces, whereas it is positive for Co/Cu, Fe/Cu, and Py/Cu. The negative and positive signs respectively found for Fe/Cr and Co/Cu interfaces are in agreement with the theoretical predictions.[34,35] For the systems investigated up to now, the same sign is generally found for the coefficient $\beta$ of an alloy $F$N and the coefficient $\gamma$ of the $F/N$ interface. This indicates some similarity between the problems of impurity scattering and electron reflections at interfaces (matching of the energy levels in $F$ and $N$ play a similar role in both problems) but this should not be a strict rule.

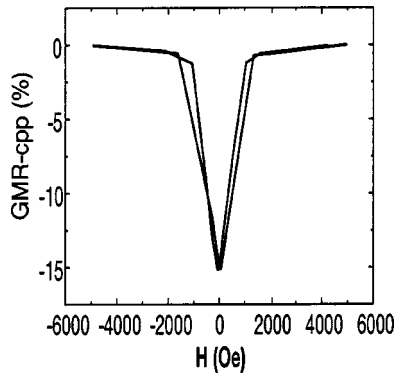


FIG. 16. Inverse GMR curve of a [$Fe$Cr 30%(5 nm)/Cr(1.1 nm)/Py(8 nm)/Cr(1.1 nm)]×20 multilayer.

## IX. WHY INVERSE GMR CAN ONLY BE RELATIVELY SMALL

The maximum value of inverse CPP-GMR we have found is 15% (Fig. 16) and, in most of our systems, the inverse GMR does not exceed 5% or 6%. This is definitely smaller than the ''normal'' CPP-GMR, 170%, for example, in Co/Cu.

The first reason of the smallness of the inverse GMR can be found in the data on the spin asymmetries in bulk materials. We can see in the extensive tables of Ref. 8, that the ratio $\alpha=\rho_\downarrow/\rho_\uparrow$ can exceed 10 in a number of alloys, whereas, when $\rho_\uparrow$ exceeds $\rho_\downarrow$, the ratio $\alpha^{-1}=\rho_\uparrow/\rho_\downarrow$ never reaches 10. This explains why, in all our ($F1/N$/Co/$N$) structures in which the inverse GMR is induced by a negative $\beta$, the GMR cannot be as large as in structures such as Co/Cu or Py/Cu with only positive spin asymmetry. Additional effects reducing the inverse GMR and explaining why the $\beta$ found in multilayers are smaller than those of bulk alloys, have already been reviewed in Sec. VII: partial compensation of the negative impurity spin asymmetry contribution by the positive spin asymmetry of the scattering by structural defects of the host, reduction of the influence of the negative spin asymmetry in doped layers by the shortening of the SDL in alloys, and stronger influence of any small departure from AP ordering in structures of the type ($F1/N/F2/N$).

In addition, for most ($F1/N/F2/N$) we have studied, there was generally a competition between bulk and interface spin asymmetries of opposite signs. In systems of the type ($F1$/Cu/Co/Cu), where $F1$ is an alloy with negative $\beta$ (example: $Ni$Cr, $Fe$V, etc.), $\gamma_{F1/Cu}$ is always positive, which leads to a partial compensation between $\beta_{F1}$ and $\gamma_{F1/N}$ (evidenced in our results by the existence of a compensation thickness). In systems of the type ($F1$/Cr/NiFe/Cr) where $F1$ is Co, CoFe, or Fe, there is a partial compensation not only between a positive $\beta_{F1}$ and negative $\gamma_{F1/Cr}$ but also between a positive $\beta_{NiFe}$ and negative $\gamma_{NiFe/Cr}$. As a matter of fact, we have obtained our highest value of inverse GMR, 15%, for ($Fe$Cr/Cr/NiFe/Cr) structures in which both $\beta_{FeCr}$ and $\gamma_{FeCr/Cr}$ are negative and do not compensate (however, there is still some partial compensation between the positive $\beta_{NiFe}$ and negative $\gamma_{NiFe/Cr}$).

## X. COMPARISON BETWEEN CIP AND CPP-GMR

In the first generation models of GMR based on spin dependent scattering of free electrons, that is, *without intrinsic potential*, the same MR ratio is predicted in the CIP and CPP geometries. In contrast, the CIP and CPP-GMR are different when an intrinsic potential is introduced. This is well illustrated, for example, by the results of Zhang *et al.*[16] who have calculated the GMR with and without intrinsic potential. Experimentally, this is also illustrated by the higher MR ratios obtained in CPP for most systems and with our ($F1/N/F2/N$) structures, by the different sign of the GMR that we have frequently found in CIP and CPP. A typical example of normal GMR in CIP and inverse in CPP is shown

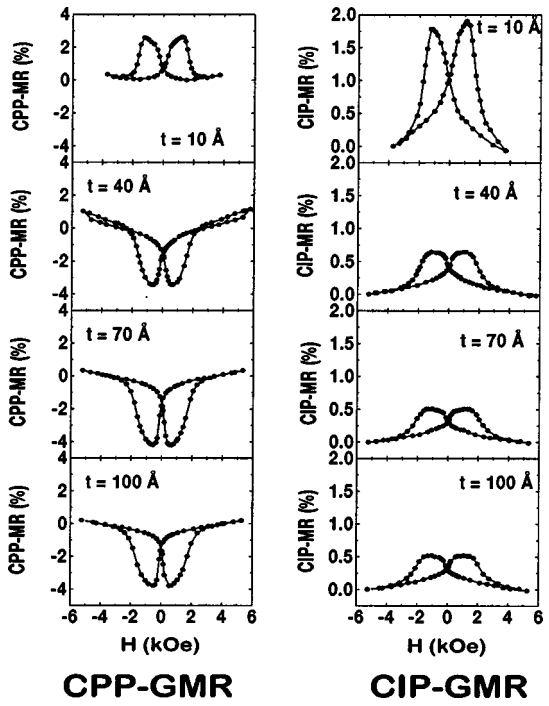


FIG. 17. Comparison between CPP-GMR (left) and CIP-GMR (right) curves for $[NiCr\ 5\%(t)/Cu(4\ nm)/Co(0.4\ nm)/Cu(4\ nm)]\times 20$ multilayers.

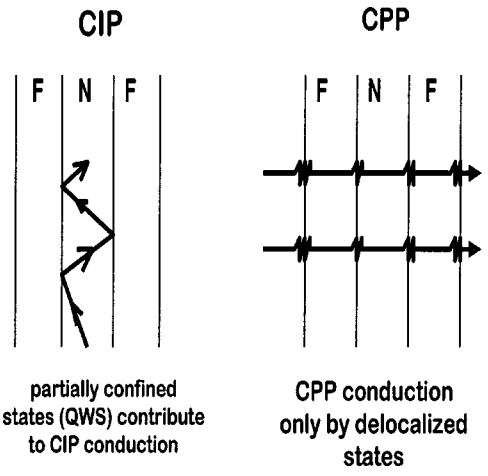


FIG. 18. Compared influence of multilayer *intrinsic potential* in CIP (left) and CPP (right). In CIP, the intrinsic potential steps at interfaces channel partially the electrons carrying the current; such channeling determines how these electrons average the extrinsic scatterings at different places in the multilayer; this mixes up the intrinsic and extrinsic effects and makes the interpretation of the GMR very complex in CIP. In CPP, the reflections by the intrinsic potential steps are expressed by spin dependent interfaces resistances (represented by zigzag); independently, the bulk scattering potentials of extrinsic origin located at different places in the multilayer (see spikes in Fig. 1) are averaged equally by the delocalized electrons carrying the CPP current. The existence of independent interface and bulk contribution makes the interpretation simpler in the CPP geometry.

in Fig 17. If we consider structures of the type $(F1/N/Co/N)$ for which we have found inverse CPP-GMR with $F1=FeCr$, $FeV$, $CoCr$, $NiCr$, and $N=Cu$, inverse CIP-GMR have been found[17,18] only for $F1=FeCr$ (planar doping), $N=Cu$, and $F1=FeV$ (with $N=Au$).

The difference between the CIP and CPP-GMR can be understood from the different role of the intrinsic potential in the two geometries as illustrated by Fig. 18. In the CPP geometry, the influence of the intrinsic potential can be expressed by its contribution to the interface resistance. The situation is different, in the CIP geometry: specular reflections of the electrons by the multilayer intrinsic potential do not contribute directly to resistance terms because the momentum along the current direction is conserved by specular reflections in CIP; however, the intrinsic potential indirectly affects conduction by channeling the electrons inside some of the layers. Zahn *et al.*[36] and Brown *et al.*[37] have described this complex situation, where the current is partly carried by delocalized electrons (nonchanneled) and partly by electrons more or less confined in normal or magnetic layers. The main result is that the confined electrons differentially probe the scattering potentials in different parts of the multilayered structure. This is in sharp contrast with the situation of the CPP geometry in which the current is carried by delocalized electrons which successively probe the scattering potentials in all layers.

These arguments can be applied, for example, to our results of Fig 17. In $(NiCr/Cu/Co/Cu)$, the inverse CPP-GMR for $t_{NiCr}>1.7$ nm is due to negative $\beta$ in $NiCr$. If, in CIP, a significant part of the current is carried by electrons partly confined in the Cu layers, these electrons will be more affected by the scattering at the $F/N$ interfaces than by bulk scattering within the ferromagnetic layers; consequently the contribution to the GMR of the negative $\beta$ will be reduced in the CIP geometry. Another source of reduction of the bulk contribution in CIP comes from the short scaling length governing the spatial variation of the electron distribution function (the mean free path, and not the SDL as in CPP). This means that, for magnetic layers thicker than the mean free path (MFP), only a depth of the order of MFP along the interfaces contributes to the CIP-GMR, whereas the inner part of the layer forms an inactive independent channel. Both effects, ''quantum channeling'' in Cu by the intrinsic potential and effective channeling induced by the shortness of the MFP, can contribute to the reduction of contribution from $\beta_{NiCr}$ in CIP and explain the results of Fig. 17. In other structures, with, for example, channeling in ferromagnetic layer, other types of effects can be expected, but, in any case, the existence of channeled currents in CIP will mean that the carriers probe the scattering potentials nonuniformly. With such mixing of intrinsic and extrinsic effects, the CIP-GMR can be hardly predicted in a simple way. The situation is much simpler in CPP, with an intrinsic contribution expressed by the interface resistance and the scattering by extrinsic potentials averaged uniformly by nonchanneled carriers.

## XI. CONCLUSIONS

In Sec. II, we have listed the current open questions in the interpretation of GMR. A number of points have been elucidated by experimental results reported in this article.

(1) The *important role of spin dependent scattering by extrinsic potentials* is illustrated by a series of experimental data on doped multilayers. These data can be clearly inter-

preted when the measurements are in the CPP geometry. It turns out that the sign and magnitude of the bulk spin asymmetry coefficient $\beta$ can be controlled by the choice of the impurities doping the ferromagnetic layers; inverse GMR effects can be obtained in $(F1/N/F2/N)$ structures by introducing spin asymmetries of different sign in $F1$ and $F2$; when the signs of the bulk and interface spin asymmetry coefficients $\beta$ and $\gamma$, are opposite in a ferromagnetic layer, there is a compensation thickness at which the GMR is zero. On the other hand, whereas the control of $\beta$ by the choice of *extrinsic* potentials is well established, the separation between the *intrinsic* and *extrinsic* contribution to $\gamma$ is not clear yet. As expected by theory,[2] it is plausible that the specular reflections by intrinsic potential steps give an important contribution to the interface parameters $r_b^*$ and $\gamma$, but it would be necessary to perform series of experiments on multilayers with controlled interface defects to estimate the additional extrinsic contribution to $r_b^*$ and $\gamma$.

(2) The second question quoted in Sec. II concerned the interpretation of the spin asymmetry coefficients $\beta$ and $\gamma$ in terms of electronic structure. For the bulk spin asymmetry coefficient $\beta$, the sign we find for various alloys is in perfect agreement with that derived from electronic structure calculations[6,7] and also in agreement with the sign found in bulk dilute alloys.[8,15] $\beta$ is positive for the pure metals Co, Ni, Fe and alloys located on the line with $-45°$ decreasing slope in the Slater-Pauling plot. $\beta$ is negative for alloys on the branches of the Slater-Pauling plot with positive slope from Ni ($Ni$Cr), Co ($Co$Cr, $Co$Mn), Fe ($Fe$Cr, $Fe$V); the classical interpretation of the negative sign, that is, $\rho_\uparrow > \rho_\downarrow$, is the existence of a resonant scattering on empty $d$ impurity states in the majority spin direction. For the contribution of interfaces, we also find positive and negative values of the spin asymmetry coefficient $\gamma$. Negative values of $\gamma$ are found for Co/Cr, Fe/Cr, $Co$Fe/Cr, and Py/Cr interfaces, while $\gamma$ is positive for all the interfaces of metal or alloys with Cu. This is in agreement with theoretical predictions. Also we find always the same sign for $\beta$ for alloys $FN$ and for $\gamma$ for an interface $F/N$, which reflects some similarity in the electronic structure in both cases but should not be a general rule.

(3) Our experiments give new examples of the important difference between the CIP and CPP GMR: not only the magnitude of the MR but also its sign can be different for measurements in CIP and CPP on the same multilayer. Models with only spin dependent scattering by extrinsic defects do not predict this difference, which emphasizes the role of the intrinsic potential. In CPP, the intrinsic potential appears through its contribution to the interface resistance parameters $r_b^*$ and $\gamma$ (the second contribution to $r_b^*$ and $\gamma$ comes from diffuse scattering by interface imperfections); *independently*, the scattering of electrons by extrinsic potentials (impurities or defects) within the layers appears in the bulk parameters $\rho^*$ and $\beta$. Once the independent bulk and interface parameters are known, the CPP GMR can be predicted. In CIP, the intrinsic potential induces channeling effects which make that the carriers probe differentially the scattering potentials at the interfaces, in the magnetic layers and in the nonmagnetic layers. This gives entwined intrinsic and extrinsic contributions and, together with the shortness of the scaling length for the damping of the electron distribution function, complicates greatly the possibility of a quantitative analysis in the CIP geometry.

What remains an open question is the respective weight of the contributions to the interface parameters $r_b^*$ and $\gamma$ which arise respectively from the intrinsic potential and from diffuse scattering by interface imperfections. We know from theory that the intrinsic contribution can be of the order of magnitude of the experimental values but we cannot rule out some significant additional contribution from diffuse scattering. Experiments similar to those on doped layers reported here but with interfaces of controlled roughness and doping would be useful to clear up this last point.

## ACKNOWLEDGMENTS

This work was supported in part by the Ford Research Laboratory, the National Science Foundation under Grant Nos. DMR 94-23795 and MRSEC 94-0017 and the MSU Center for Fundamental Materials Research. A.F. acknowledges support through the NEDO program of Japan (International Joint Project ''Spin-dependent quantum effects in artificial nanostructures and spin devices'').

[1] For a review of theoretical models, see P.M. Levy, *Solid State Physics* (Academic, New York, 1994), Vol. 47, p. 367.

[2] K.M. Schep, J.B.A.N. van Hoof, P.J. Kelly, G.E.W. Bauer, and J.E. Inglesfield, Phys. Rev. B **56**, 10 805 (1997).

[3] T. Valet and A. Fert, Phys. Rev. B **48**, 7099 (1993).

[4] S.Y. Hsu, A. Barthélémy, P. Holody, R. Loloee, P.A. Schroeder, and A. Fert, Phys. Rev. Lett. **78**, 2652 (1997).

[5] C. Vouille, A. Fert, A. Barthélémy, S.Y. Hsu, R. Loloee, and P.A. Schroeder, J. Appl. Phys. **81**, 4573 (1997).

[6] I. Mertig, R. Zeller, P.H. Dederich, Phys. Rev. B **47**, 16 178 (1993).

[7] V.Y. Irkhin and Y.P Irkhin, J. Magn. Magn. Mater. **164**, 1191 (1996).

[8] A. Fert and I.A. Campbell, J. Phys. F **6**, 840 (1976).

[9] R.E. Camley and J. Barnas, Phys. Rev. Lett. **63**, 664 (1989).

[10] P.M. Levy, S. Zhang, and A. Fert, Phys. Rev. Lett. **65**, 1643 (1990).

[11] See, for example, Ref. 4. Interface resistances have also been calculated by J. Barnas and A. Fert, Phys. Rev. B **49**, 12 835 (1994); J. Magn. Magn. Mater. **136**, 260 (1994); V.K. Dugaev, V.I. Lituinov, and P.P. Petrov, Phys. Rev. B **52**, 5306 (1995).

[12] S.F. Lee, W.P. Pratt, Jr., Q. Yang, P. Holody, R. Loloee, P.A. Schroeder, and J. Bass, J. Magn. Magn. Mater. **110**, L1 (1993).

[13] W.P. Pratt, Jr., S.F. Lee, Q. Yang, P. Holody, R. Loloee, P.A. Schroeder, and J. Bass, J. Appl. Phys. **73**, 5326 (1993).

[14] J.L. Duvail, A. Barthélémy, L.B. Steren, R. Morel, F. Petroff, M. Sussiau, M. Wiedemann, A. Fert, P. Holody, R. Loloee, and P.A. Schroeder, J. Magn. Magn. Mater. **151**, 324 (1995).

[15] Dorleign and Miedema, in *Magnetism and Magnetic Materials*, Proceedings of the First Joint MMM-Intermag Conference,

Pittsburgh, 1976, AIP Conf. Proc. No. **34**, edited by J. J. Becker and G. H. Lander (AIP, New York, 1976).

[16] S. Zhang and P.M. Levy, in *Magnetic Ultrathin Films—Multilayers and Surfaces, Interfaces and Characterization*, edited by B. T. Jonker *et al.*, MRS Symposia Proceedings No. 313 (Materials Research Society, Pittsburgh, 1993), p. 53.

[17] J.M. George, L.G. Pereira, A. Barthélémy, F. Petroff, L.B. Steren, J.L. Duvail, A. Fert, R. Loloee, P. Holody, and P.A. Schroeder, Phys. Rev. Lett. **72**, 408 (1994).

[18] J.P. Renard, P. Bruno, R. Megy, B. Bartenlian, P. Beauvillain, C. Chappert, C. Dupas, E. Kolb, M. Mulloy, P. Veillet, and E. Velu, Phys. Rev. B **51**, 12 821 (1995).

[19] R.K. Nesbet, J. Phys.: Condens. Matter **6**, 449 (1994).

[20] W.H. Butler, X.G. Zhang, D.M.C. Nicholson, and J.M. Mac Laren, Phys. Rev. B **52**, 13 399 (1995).

[21] J.M. Slaughter, W.P. Pratt, Jr., and P.A. Schroeder, Rev. Sci. Instrum. **60**, 127 (1989).

[22] S.F. Lee, Q. Yang, P. Holody, R. Loloee, J.H. Hetherington, S. Mahmood, B. Ikegami, K. Vigen, L.L. Henry, P.A. Schroeder, W.P. Pratt, Jr., and J. Bass, Phys. Rev. B **52**, 15 426 (1995).

[23] W.P. Pratt, Jr., S.F. Lee, J.M. Slaughter, R. Loloee, P.A. Schroeder, and J. Bass, Phys. Rev. Lett. **66**, 3060 (1991).

[24] P. Holody, L.B. Steren, R. Morel, A. Fert, R. Loloee, and P.A. Schroeder, Phys. Rev. B **50**, 12 999 (1994).

[25] L. Piraux, S. Dubois, and A. Fert, J. Magn. Magn. Mater. **159**, L287 (1996); L. Piraux, S. Dubois, A. Fert, and L. Belliard, Eur. Phys. J. B **4**, 413 (1998).

[26] W.P. Pratt, Jr., S.D. Steenwyck, S.Y. Hsu, W.C. Chiang, A.C. Schaefer, R. Loloee, and J. Bass, IEEE Trans. Magn. **33**, 3505 (1997).

[27] A. Fert, J.L. Duvail, and T. Valet, Phys. Rev. B **52**, 6513 (1995); Q. Yang, P. Holody, S.F. Lee, L.L. Henry, R. Loloee, P.A. Schroeder, W.P. Pratt, and J. Bass, Phys. Rev. Lett. **72**, 3274 (1994).

[28] P. Monod and S. Schultz, J. Phys. (France) **43**, 393 (1982).

[29] S.Y. Hsu, P. Holody, R. Loloee, J.M. Rittner, W.P. Pratt, Jr., and P.A. Schroeder, Phys. Rev. B **54**, 9027 (1996).

[30] W. Park, R. Loloee, J. Caballero, W.P. Pratt, Jr., P.A. Schroeder, J. Bass, C. Vouille, and A. Fert, J. Appl. Phys. **85**, 1 (1999).

[31] Q. Yang, P. Holody, R. Loloee, L.L. Henry, W.P. Pratt, Jr., P.A. Schroeder, and J. Bass, Phys. Rev. B **51**, 3226 (1995).

[32] A.C. Reilly, R. Slater, B. Ouaglal, W.P. Pratt, Jr., and J. Bass, J. Magn. Magn. Mater. **195**, 269 (1999).

[33] P. Holody, W.C. Chiang, R. Loloee, J. Bass, W.P. Pratt, Jr., and P.A. Schroeder, Phys. Rev. B **58**, 12 230 (1998).

[34] R.K. Nesbet, J. Magn. Magn. Mater. **159**, L17 (1996).

[35] W.H. Butler, X.G. Zhang, T.C. Schulthess, D.M.C. Nicholson, J.M. Mac Laren, V.S. Speriosu, and B.A. Gurney, Phys. Rev. B **56**, 14 574 (1997).

[36] P. Zahn, J. Binder, I. Mertig, R. Zeller, and P.H. Dederichs, Phys. Rev. Lett. **80**, 4309 (1998).

[37] R.H. Brown, D.M.C. Nicholson, W.H. Butler, X.G. Zhang, W.A. Shelton, T.C. Schulthess, and J.M. Mac Laren, Phys. Rev. B **58**, 11 146 (1998).